Research, Society and Development, v. 12, n. 1, e29912139831, 2023
(CC BY 4.0) | ISSN 2525-3409 | DOI: http://dx.doi.org/10.33448/rsd-v12i1.39831

Lagrangian reconciliation of expeditious analyzes on microflotation of hematite and dolomite by carboxylates

Reconciliação lagrangeana de análises expeditas na microflotação de hematita e dolomita por carboxilatos

Reconciliación lagrangiana de análisis expeditos en microflotación de hematita y dolomita por carboxilatos

Received: 12/29/2022 | Revised: 01/09/2023 | Accepted: 01/10/2023 | Published: 01/12/2023

Bruna de Oliveira Gomes
ORCID: https://orcid.org/0000-0003-0627-5542
Universidade Federal de Ouro Preto, Brazil
E-mail: bruna.ogomes@hotmail.com
Fernanda Bento Sales
ORCID: https://orcid.org/0000-0002-5586-1751
Universidade Federal de Ouro Preto, Brazil
E-mail: Fernanda.sales1@aluno.ufop.edu.br
José Aurélio Medeiros da Luz
ORCID: https://orcid.org/0000-0002-7952-2439
Universidade Federal de Ouro Preto, Brazil
E-mail: jaurelio@ufop.edu.br
Felipe de Orquiza Milhomem
ORCID: https://orcid.org/0000-0002-9830-8374
Universidade Federal do Mato Grosso, Brazil
E-mail: felipe.milhomem6@gmail.com

Abstract
Microflotation campaign of a synthetic binary mixture of hematite and dolomite was carried out in order to evaluate the potential of saponified cottonseed oil as a collector. Hematite content was determined by expeditious methods, namely image analysis, pycnometry, and carbonate thermolysis by calcination. An algebraic reconciliation algorithm of redundant data (via Lagrange multipliers) was developed to treat the raw data from the different analytical techniques, aiming to increase the accuracy of the results, with the additional piece of information arising from product weighing, by introducing a dummy variable. At the stage of the study reported here, the physicochemical conditions for the selective flotation of hematite were not optimized; however, the results showed potential (both under acid and alkaline conditions) for the selective anionic flotation of the hematite/dolomite system. Prospective tests evaluating the analytical techniques employed showed pycnometry and calcination tended to be more reliable methods. Although the imaging method has shown promise, it still lacks some improvement in procedure for greater accuracy. The minimization of closure errors in mass balancing by using the mentioned optimization algorithm under constraints showed to be very relevant for the adequate evaluation of the separation process, using very small samples, as in the case of microflotation.
Keywords: Fuerstenau cell; Cottonseed oil; Quick analysis; Lagrange multipliers.

Resumo
Campanha de microflotação duma mistura binária sintética de hematita e dolomita foi realizada a fim de avaliar o potencial do óleo de semente de algodão saponificado como coletor. O teor de hematita foi determinado por métodos expeditos, a saber: análise de imagem, picnometria e termólise de carbonato por calcinação. Um algoritmo de reconciliação algébrica de dados redundantes (via multiplicadores de Lagrange) foi desenvolvido para tratar os dados brutos obtidos pelas diferentes técnicas analíticas, visando a aumentar a precisão dos resultados, com a inclusão adicional de informação consubstanciada pelas pesagens dos produtos, através da introdução de variável virtual. No estágio do estudo aqui relatado não se otimizaram as condições físico-químicas para a flotação seletiva de hematita; entretanto os resultados mostraram potencial (tanto sob condições ácidas, quanto alcalinas) na flotação aniônica seletiva do sistema hematita/dolomita. Ensaios prospectórios de avaliação das técnicas analíticas empregadas mostraram que os picnometria e calcinação tendem a ser métodos mais confiáveis. O imageamento digital, embora tenha se mostrado promissor, carece ainda de melhoria no procedimento, para maior acurácia. A minimização dos erros de fechamento do balanço de massas pelo empreso do citado algoritmo de otimização sob vínculos mostrou-se muito relevante para a adequada avaliação do processo de separação empregando amostras diminutas, como no caso da microflotação.
Palavras-chave: Célula de fuerstenau; Óleo de caroço de algodão; Análise simplificada; Multiplicadores de lagrange.

Resumen
Se llevó a cabo una campaña de microflotación de una mezcla binaria sintética de hematita y dolomita para evaluar el potencial del aceite de semilla de algodón saponificado como colector. El contenido de hematita se determinó mediante métodos expeditos, a saber, análisis de imágenes, picnometría y termólisis de carbonatos por calcinación. Se desarrolló un algoritmo de reconciliación algebraica de datos redundantes (via multiplicadores de Lagrange) para tratar los datos brutos procedentes de las distintas técnicas analíticas, con el objetivo de aumentar la precisión de los resultados, con la información adicional derivada del pesaje del producto, mediante la introducción de una variable virtual. En la etapa del estudio aquí relatada, las condiciones fisicoquímicas para la flotación selectiva de la hematita no fueron optimizadas; sin embargo, los resultados mostraron potencial (tanto en condiciones ácidas como alcalinas) para la flotación aniónica selectiva del sistema hematites/dolomita. Unos experimentos prospectivos de evaluación de las técnicas analíticas empleadas mostraron que la picnometría y la calcinación tendían a ser métodos más fiables. Aunque el método de análisis de imágenes se ha mostrado prometedor, todavía carece de algunas mejoras en el procedimiento para una mayor precisión. La minimización de errores de cierre en el balance de masas mediante el uso del mencionado algoritmo de optimización bajo restricciones demostró ser muy relevante para la adecuada evaluación del proceso de separación, utilizando muestras muy pequeñas, como en el caso de la microflotación.
Palabras clave: Celda de fuerstenau; Aceite de semilla de algodón; Análisis expedito; Multiplicadores de lagrange.

1. Introduction

Vegetable oils (having triacylglycerols as their major components) have been used in several industrial applications due to their low toxicity to humans and the environment, they come from renewable resources and are inherently biodegradable (Erhan, 2005). In mineral processing, fatty acid salts from vegetable oils are already widely studied as collectors as anionic flotation processes are concerned (Leja, 2004; Brandão *et al.*, 1994).

Vieira *et al.* (2005) investigated the performance of a few vegetable oils as collectors in calcite microflotation: castor oil (*Ricinus communis*), palm oil (*Cocos nucifera*), pequi (*Caryocar brasiliense*) and sesame oil (*Sesamum indicum*). In turn, Costa (2012) evaluated oils from buriti (*Mauritia flexuosa*), passion fruit seed (*Passiflora edulis*), inajá (*Attalea maripa*), Brazil nut (*Bertholletia excelsa*), andiroba seed (*Carapa guianensis*) and açaí (*Euterpe oleracea*) pulp as collectors in phosphate ore flotation. Silva *et al.* (2015) studied the use of pequi oil in apatite flotation. Milhomem (2020) evaluated the applicability of mango (*Mangifera indica*), pequi and palm oils in the microflotation of hematite (Fe_2O_3) and quartz (SiO_2).

In order to evaluate the performance of vegetable oils on flotation, it is necessary to carry out experimental campaigns on an increasing scale which, according to Chudacek *et al.* (1992), is divided into three methods, namely: microflotation, bench cells and pilot plants.

The main purpose of microflotation tests is to understand the mechanisms of interaction between minerals and reagents, leading to the definition of the best physicochemical conditions of the system (Luz, 1996). Nevertheless, forecasting technical operational indicators, such as metallurgical recovery, product contents, and Gaudin's selectivity index, is — at this early stage of process route development — only a secondary goal, if at all.

Microflotation studies are commonly carried out under controlled physicochemical and fluid dynamic conditions in simplified systems, to better highlight the interactions between reactants and mineral surfaces. Furthermore, it is difficult to determine the mineral contents in a system with a mixture of minerals due to the low mass used or even the lack of resources. Especially in the case of using a Hallimond tube (Leja, 2004; Drzymala, 1994a; Drzymala, 1994b), which typically uses samples of 0.001 kg (1.0 g). In contrast, the use of a Fuerstenau cell (Fuerstenau, 1964; Luz, 1996) less dramatic, since it typically employs about 0.0020 kg (20.0 g) per experiment.

Milhomem (2020) carried out microflotation tests with synthetic mixtures of hematite and quartz, using a Fuerstenau cell (employing total sample mass of 24.00 g). Magnetic separation with a rare-earth magnet and measurement of the specific mass with a helium pycnometer were used to evaluate the content of the floated material, thus allowing the estimation of the process performance.

Although laboratories of large organizations have enough equipment to determine the content of minerals, many laboratories of more modest enterprises do not use sophisticated instrumental methods for this, making the use of expeditious methods extremely convenient to obtain the desired information, even if, as a counterpart, there is a loss of accuracy of the quantifications. A promising technique is image analysis, which, until recently, required, as a rule, sophisticated instruments (Milhomem & Luz, 2018).

Milhomem and Luz (2018) evaluated an accessible method to determining mineral content through colorimetry in an educational laboratory using cell phones. Synthetic mixtures samples of hematite and quartz granules were used for the evaluation, using the so-called color index, allowing the prediction of the proportion of hematite in mixtures with optically contrasting materials. The analyzes were performed using two Android applications: *Color Meter* from VisTech Projects and *Color Analysis* from Research Lab Tool, both presenting results in line with the additive system of RGB colors. This approach has shown to be promising in the context of using very low-cost and easy-to-execute methods.

In a similar approach, Neuppmann (2019) also quantified the hematite and quartz contents of microflotation through image analysis. The quantification consisted of analyzing pixel histograms generated by the *IrfanView*® software. First, a calibration curve employing binary mixtures with controlled quartz proportions was constructed, using a cheap digital microscope (with USB connection) to take the images. Subsequently, in sequence, an algorithm based on the use of Lagrange multipliers with the inclusion of a virtual (dummy) variable was used, according to the procedure recommended by Luz (1999), to add the informational load from the mass balance itself (via the weighing of the test products). This virtual component had its fictitious grades chosen in such a way as to numerically reproduce the mass recovery from the scale measurements. Their results indicated coefficient of determination (the linear correlation coefficient squared) of 95.99 % with respect to the experimental data cloud.

Hematite (Fe_2O_3) and dolomite ($CaMg(CO_3)_2$) are two minerals that present divergent features, not only in terms of color, but also in density, and mass calcination loss. Naturally, the decomposition of carbonates at high temperatures, with the release of carbon dioxide, results in a substantially greater loss than that experienced by hematite, which, when pure and dry, has zero loss. Considering the pure composition of the double carbonate, dolomite has a molecular mass equal to 0.18440 kg; the complete thermal decomposition (thermolysis) yields 30.41 % CaO; 21.86 % MgO and 47.73 % CO_2, according to the following reactions (Aliyu1 *et al*., 2022; Sampaio & Almeida, 2008):

$$CaMg(CO_3)_2 \rightarrow MgO + CaCO_3 + CO_2 \quad [\Delta Hr = +117 \text{ kJ/mol}] \tag{A}$$

$$CaMg(CO_3)_2 \rightarrow MgO + CaO + 2\,CO_2 \quad [\Delta Hr = +164 \text{ kJ/mol}] \tag{B}$$

In the precedent reactions the figures inside the square brackets are the endothermic enthalpy of reaction.

However, due to impurities containing hydroxyls or water of constitution (or even adsorbed water from air), heating often results in the evolution of these volatile constituents (generally minor losses). This aspect is relevant when dealing with hydrated iron mineralogical phases, such as goethite. In the occurrence of magnetite, heating in kilns without atmosphere control can falsify the results, due to the addition of oxygen in the sample, resulting from the magnetite oxidation. All these aspects emphasize the convenience of combining pycnometry, imaging, and calcination information.

This article aimed to highlight the use of algebraic techniques to gain accuracy in mass balancing, applied to systems where the samples are very small, greatly hindering the potential of conventional analytical techniques, as occurs in microflotation. To contextualize the problem, the potential of saponified cottonseed oil as an anionic collector in the selective flotation of the hematite/dolomite system was prospectively selected as an example that points out possible technological novelty.

2. Materials and Methods

The particle size adjustment of the dolomite was performed using a ball mill and the classification was done by wet sieving, using the samples whose sizes are between 212 µm and 105 µm. In order to increase the purity of the hematite material, the sample was subjected to wet magnetic separation and the magnetic concentrate used in the subsequent assays. Regression analysis of the hematite particle size distribution was performed using the *Easyplot*® software. The cumulative distributions studied were those from Rosin–Rammler, Gates–Gaudin–Schumann, Hill, Gaudin–Meloy, and Harris.

The thermal decomposition of the samples was determined by thermogravimetric analysis (TG) and its derivative. Thermogravimetric analysis was carried out employing a thermobalance Model TGA Q50 V20.10, from Quantachrome Instruments. Heating ramp was 0.166 K/s, ranging from room temperature up to 1,273.1 K in nitrogen atmosphere under flow rate of 1.66 x 10^{-6} m^3/s. X-ray diffractometry (total powder method) was performed with a X'Pert3 Powder diffractometer from Malvern Panalytical, using a copper anode tube ($\lambda = 1.5406 \times 10^{-10}$ m), under 45 kV of potential difference, 40 mA current, with angular scanning from 5º to 90º. About 50 g of sample were previously comminuted in an orbital ring and cylinder pulverizer. The diffractogram was generated by *Data Collector* software and interpreted using *Highscore Plus* software, which performs a Rietveld refinement.

The microflotation assays were carried out in a Fuerstenau cell (Figure 1) only with the collectors at a concentration of 20 mg/L, in duplicate, with 0.024 kg of a mixture of minerals (being 12 g of each), and with an initial pH of 5.0, 6.1, 7.2, 8.3, and 9.4. All tests were performed in duplicate. Experiments with depressants have not been carried out.

Figure 1 — Fuerstenau cell (1 — stopcock for gas injection; 2 — porous plug (glass frit); 3 — cell supported by clamps; 4 — froth overflow; 5 — mechanical impeller axis).

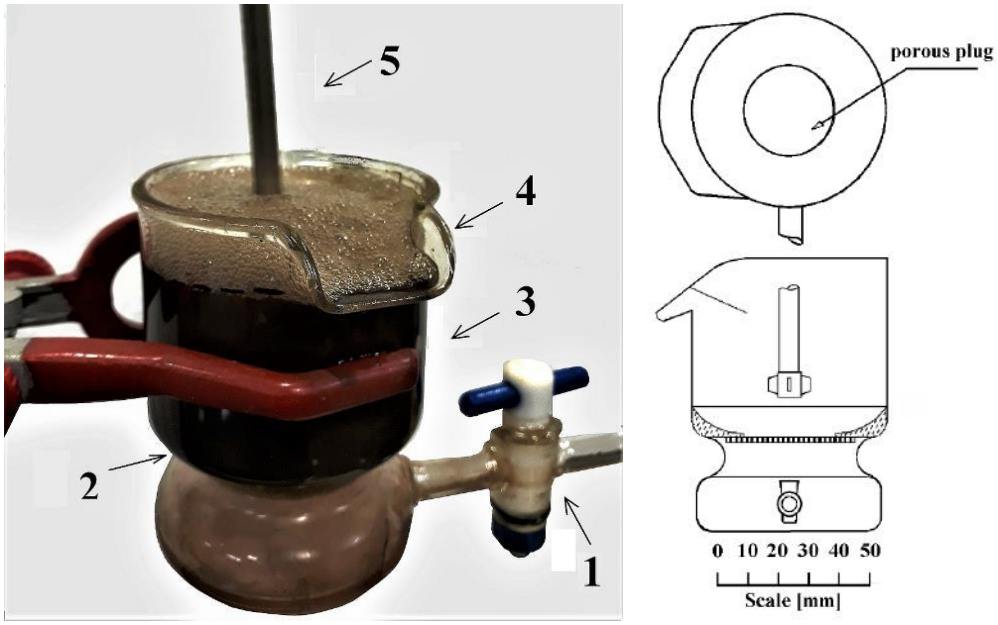

Source: Authors' own elaboration.

Before applying the image analysis method to the microflotation samples, a calibration curve was constructed with methodology based on the work of Neuppmann (2019). Aliquots of 0.0001 kg (0.1 g) of binary mixture of hematite and dolomite were used in the following proportions of hematite: 0 %, 10 %, 20 %, 30 %, 40 %, 50 %, 60 %, 70 %, 80 %, 90 %, and 100 %.

The samples were weighed in a Petri dish and as the samples contain binary mixture, it was necessary to separate the minerals to facilitate the image analysis. For this purpose, a vibrating table was used which, due to the difference in density, made the dolomite particles separate more easily. After this process, the most detailed scattering of the particles was carried out with light taps on the side of the Petri dish. Subsequently, some photos were taken using a smartphone and a light table to avoid shadows in the images.

Using the *IrfanView*® software, the image background was converted to red, the hematite particles to black and the dolomite particles to white dots. A pixel histogram was generated indicating the percentage of the three colors. Figure 2 shows an example of particle spreading on Petri dish and the image obtained after color treatment.

Figure 2 — Example of: a) particle dispersion and b) the image after color treatment.

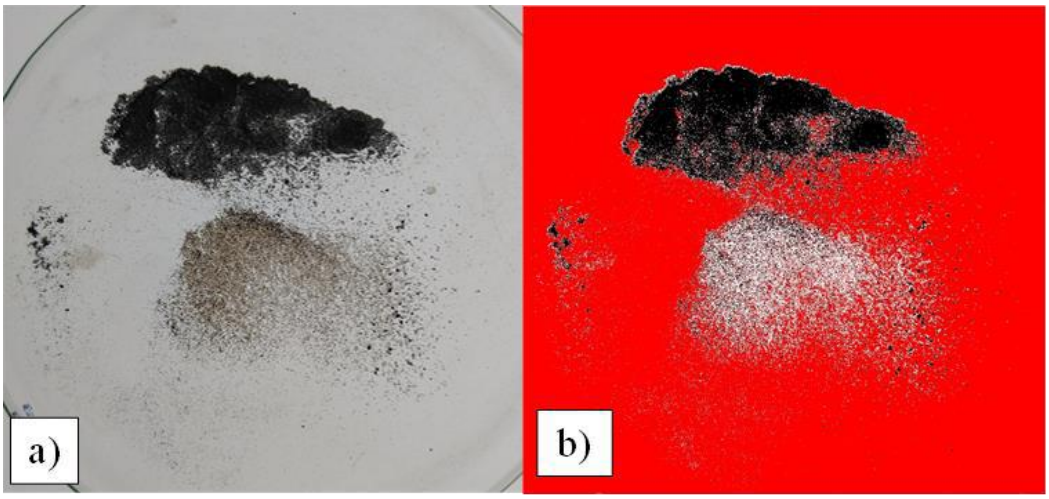

Source: Authors' own elaboration.

The grade of each mineral was calculated using Equation 1:

$$t_{m1} = \frac{c_{m1}}{c_{m1} + c_{m2}} \quad (1)$$

Where: t_{m1} — grade (content) of mineral ***1*** in sample [–]; c_{m1} — mass fraction of mineral ***1*** (from the proportion of projected area inferred from the pixel histogram, after image binarization) [–]; c_{m2} — mass fraction of mineral ***2*** (from the proportion of projected area inferred from the pixel histogram, after image binarization) [–].

The samples resulting from microflotation underwent the image analysis process whose applied methodology was the same described above. Subsequently, the levels were determined by the pycnometry method.

The grade by pycnometry was determined using the Gay-Lussac water pycnometer method, without Archimedean thrust correction (as recommended by Shoemaker *et al.* (1996), for extra high accuracy determination). After determining the density of the material, the grade of each mineral was calculated using Equation 2:

$$t_{m1} = \frac{\rho_{m1}(\rho_T - \rho_{m2})}{\rho_T(\rho_{m1} - \rho_{m2})} \quad (2)$$

Where: t_{m1} — grade (content) of mineral ***1*** in sample [–]; ρ_{m1} — density (specific mass) of mineral ***1*** [kg/m³]; ρ_{m2} — density (specific mass) of mineral ***2*** [kg/m³]; ρ_T — density (specific mass) of mineral mixture [kg/m³].

Historical data on density determination by water pycnometry have revealed that the good estimate of uncertainty for this technique (in terms of relative error) was 0.177 %.

Once the densities were determined, the dried pycnometry samples were poured into properly labeled crucibles and calcined at 1,173 K (900°C) using a muffle kiln for 10,800 s (3 hours). The grade of each mineral was calculated according to the mass loss of the thermolysis process, using Equations 3, 4 and 5:

$$t_d = \frac{q - f_h}{f_d - f_h} \quad (3)$$

$$q = \frac{m_f}{m_i} \quad (4)$$

$$t_h = 1 - t_d \quad (5)$$

Where: t_d — dolomite grade in sample [–]; q — residual fraction after calcination [–]; m_i — initial mass before calcination [kg]; m_f — final mass after calcination; f_h — residual mass fraction of hematite inferred from the thermogravimetric assay [–]; f_d — mass residue of dolomite inferred from the thermogravimetric assay; t_h — hematite grade in sample [–].

The data were applied in a mathematically redundant data matching algorithm, based on minimization under constraints using Lagrange multipliers (Wills, 2006; Vasebi *et al.*, 2012; Hodouin, 2010), with inclusion of a virtual variable (according preconized by Luz, 1999). In the present case the virtual variable chosen had dummy contents adopted in such a way as to be numerically compatible with the mass recovery from weighing the products. Knowing that the effective grade of the feed was 50.00 % (by sample preparation) and choosing the concentrate content equal to that obtained by pycnometry (which was the more accurate method) for hematite, the value of the tailings content that was compatible with that known mass recovery. That is, according to the equation (Luz, 1999):

$$t^* = \frac{(f^* - c^* \times R^*_{mas})}{(1 - R^*_{mas})} \quad (6)$$

In precedent equation, t^*, f^*, c^* and R^*_{mas} stand for, respectively, tailing, feed (50 %), concentrate (the same figures of hematite from pycnometry), and mass recovery (from scale weighting) for the dummy variable.

With the results of the floated and non-floated grades of each method, values of relative error of the feed were calculated as 0.04 %, related to the relative error from the precision balance. Due to the lack of adequate historical series, the approximate relative error, referring to calcination tests was 3 %, for the pycnometry was 1.77 % and for the image analysis 4 %. In turn, since the hematite content in non-floated concerning the dummy variable is a rational type of function (as can see in Equation 6) the relative error associated with this parameter was calculated by the following equation:

$$\frac{\sigma_{t^*}}{t^*} = \sqrt{\left(\frac{\sigma_{f^*}}{f^*}\right)^2 + \left(\frac{\sigma_{c^*}}{c^*}\right)^2 + \left(\frac{\sigma_{R^*_{mass}}}{R^*_{mass}}\right)^2} \quad (7)$$

The Greek letter sigma above stands for standard deviation. The estimate adopted for the relative error of dummy tailing content, taking into account the preceding equation was 0.15 %.

The adjusted mass recovery was calculated by Equation 8.

$$R_{mass} = \frac{\sum_{i=1}^{n}(f_i - t_i).(c_i - t_i)}{\sum_{i=1}^{n}(c_i - t_i)} \quad (8)$$

Where: R_{mass} — adjusted mass recovery [–]; f_i — hematite grade in the feed from analytical method i [–]; t_i —hematite grade in not floated product from analytical method i [–]; c_i — grade of floated hematite from the analytical method i [–].

Subsequently, the adjusted grades were calculated by subtracting the raw contents by the adjustment values for all flows (feed, floated and non-floated) that are obtained through Equations 9, 10 and 11.

$$\delta_f(i) = \frac{[f_i - R_{mass}.c_i - (1 - R_{mass}).t_i]}{1 + R_{mass}^2 + (1 - R_{mass})^2} \quad (9)$$

$$\delta_c(i) = \frac{-\{R_{mass}[f_i - R_{mass}.c_i - (1 - R_{mass}).r_i]\}}{1 + R_{mass}^2 + (1 - R_{mass})^2} \quad (10)$$

$$\delta_t(i) = \frac{-\{(1 - R_{mass})[f_i - R_{mass}.c_i - (1 - R_{mass}).t_i]\}}{1 + R_{mass}^2 + (1 - R_{mass})^2} \quad (11)$$

Where: $\boldsymbol{\delta_f\ (i)}$ — feed adjustment value for method i; $\boldsymbol{\delta_c\ (i)}$ — float adjustment value for method i; $\boldsymbol{\delta_t\ (i)}$ — non-float adjustment value for method ***i***.

To enhance the analysis of the microflotation results, the Gaudin selectivity index and the metallurgical recovery of each test were obtained through Equations 13 and 14.

The Gaudin's selectivity index (SI) is the geometric mean between the worthy constituting recovery and gangue rejection and can be calculated by the Equation 13 (Gaudin, 1975; Luz, 2016).

$$SI = \sqrt{\frac{c}{c_{gangue}} \times \frac{t_{gangue}}{t}} \quad (13)$$

The following nomenclature applies in the preceding equation: ***c*** — content of the valuable component in the concentrate [–]; $\boldsymbol{c_{gangue}}$ — content of the gangue in the concentrate [–]; ***t*** — content of the valuable component in tailing [–]; $\boldsymbol{t_{gangue}}$ – content of the gangue in tailing [–].

The metallurgical recovery can be calculated by the Equation 14 (Gaudin, 1975; Wills & Napier–Munn, 2006; Luz, 1996).

$$R = \frac{c\ (f - t)}{f\ (c - t)} \quad (14)$$

Where: ***f*** — hematite grade in the feed [–]; ***t*** — hematite grade in tailings [–]; ***c*** — hematite grade in concentrate [–].

3. Results and Discussion

3.1 Mineral characterization

The Figure 3 presents the values of the size distribution of the hematite (cumulative passing through). The results show $\boldsymbol{d_{80}}$ of 76.08 μm and one can observe that the material is practically free of slimes (particles less than 10 μm).

Figure 3 — Size distribution of the hematite.

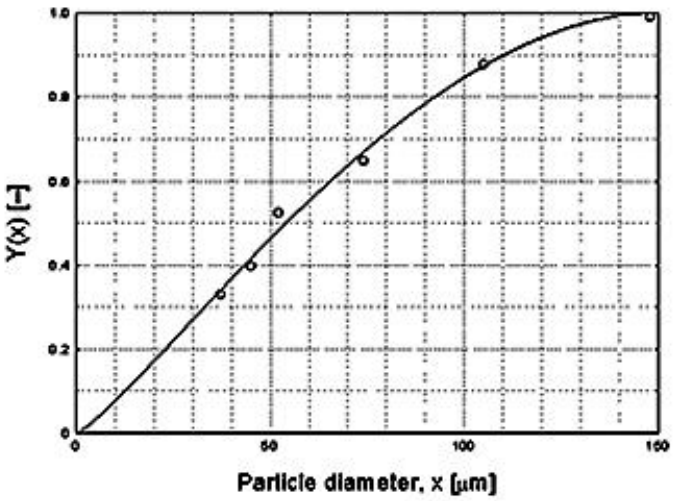

Source: Authors' own elaboration.

Harris distribution has shown higher goodness-to-fit for the particle size data (solid line in Figure 3), and the coefficient of determination (the linear correlation coefficient squared) for this regression was $\boldsymbol{R}^2 = 0.99174$. The resulting equation is:

$$Y = 1 - \left[1 - \left(\frac{x}{x_{max}}\right)^{a}\right]^{b} = 1 - \left[1 - \left(\frac{x}{148\ \mu m}\right)^{1.8178}\right]^{1.2026} \quad (12)$$

The Figures 4 shows the thermogram for the hematite sample under inert atmosphere, depicting both the relative mass loss with the progress of heating, as its derivative in time.

Figure 4 — Thermogram of the hematite sample.

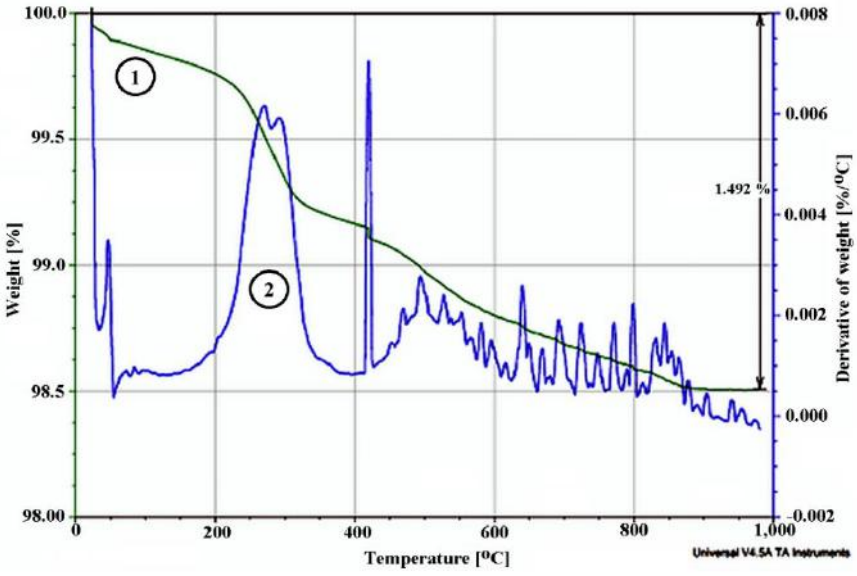

Source: Authors' own elaboration (modified from the instrument output).

The curve of the thermogravimetric analysis of hematite shows a process of mass loss (curve 1, in green), possibly related to the release of volatile matter from the sample until approximately 523.1 K (250 °C), with a mass loss around 0.31%. The derivative curve (curve 2, in blue) shows two peaks associated with this process, at temperatures of 303.1 K (30 °C) and 323.1 K (50°C). This mass loss may correspond to the elimination of water, physically bound by van der Waals forces and kept by hydrogen bonding (Rocha *et al.*, 2009; Souza *et al.*, 2020).

Another mass loss of 0.56 % occurs in the range from 523.1 K (250 °C) to 698.1 K (425 °C), with peaks between 548.1 K (275 °C) and 573.1 K (300 °C) and another at 698.1 K (425 °C) in the derivative curve. This mass decrease corresponds to the loss of hydroxyl, which indicates the possible presence of goethite in the sample that, according to Leonel (2011) and Salama *et al.* (2015), its dehydroxylation occurs in the range of 499.1 to 698.1 K (226 to 425 °C).

According to Rocha (2008), the mass loss in the range of 773.1 to 873.1 K (500 to 600 °C) may be related to the loss of hydroxyls from clay minerals, therefore, the loss of hematite from 698.1 K (425 °C) onwards may be related to this phenomenon.

According to Millan *et al.* (2016), two mass losses are expected in dolomite samples (curve 3, in green) related to decarbonation of its constituents, the first being of $MgCO_3$ between 673.1 and 873.1 K (400 and 600 °C) and the second of $CaCO_3$ between 873.1 and 1176.1 K (600 and 900 °C). During the process, water loss from hydroxyls can occur in clay minerals processing around 758.1 K (485 °C) (Soares *et al.*, 2014) and/or in the range of 773.1 to 873.1 K (500 to 600 °C) (Rocha, 2008).

Figure 5 — Thermogram of the dolomite.

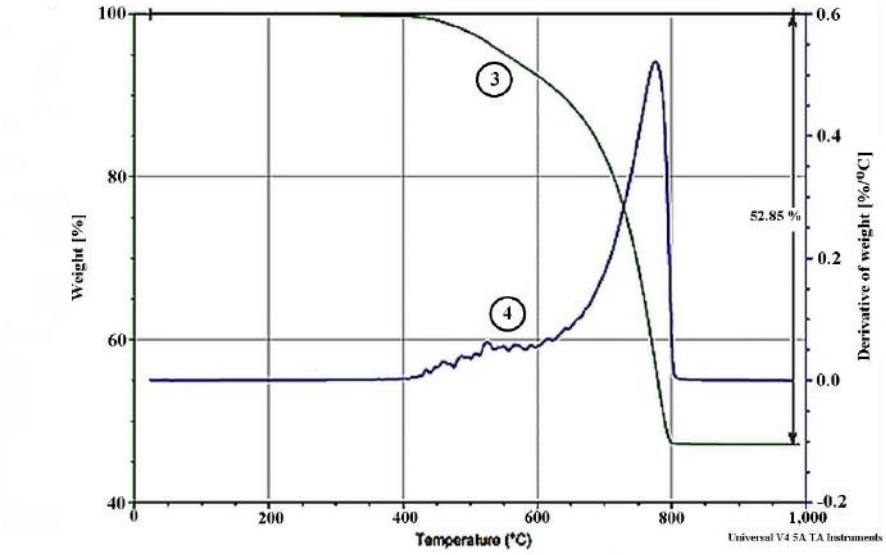

Source: Authors' own elaboration (modified from the instrument output).

These phenomena can be observed in Figure 5, especially between 873.1 and 1073.1 K (600 and 800 °C), where the largest peak in the derivative curve (curve 4, in blue) can be noted. Between 673.1 and 873.1 K (400 and 600 °C) there is a lower mass loss, which may be related to the amount of $MgCO_3$ present in the sample or even due to other components, such as clay minerals. The whole process resulted in a total mass loss of 52.85 %.

In turn, Figure 6 shows the X-ray diffractogram for the iron ore sample, which identified the presence of the following mineral phases: goethite, hematite, quartz and kaolinite.

Figure 6 — X-ray diffraction analysis of the hematite sample.

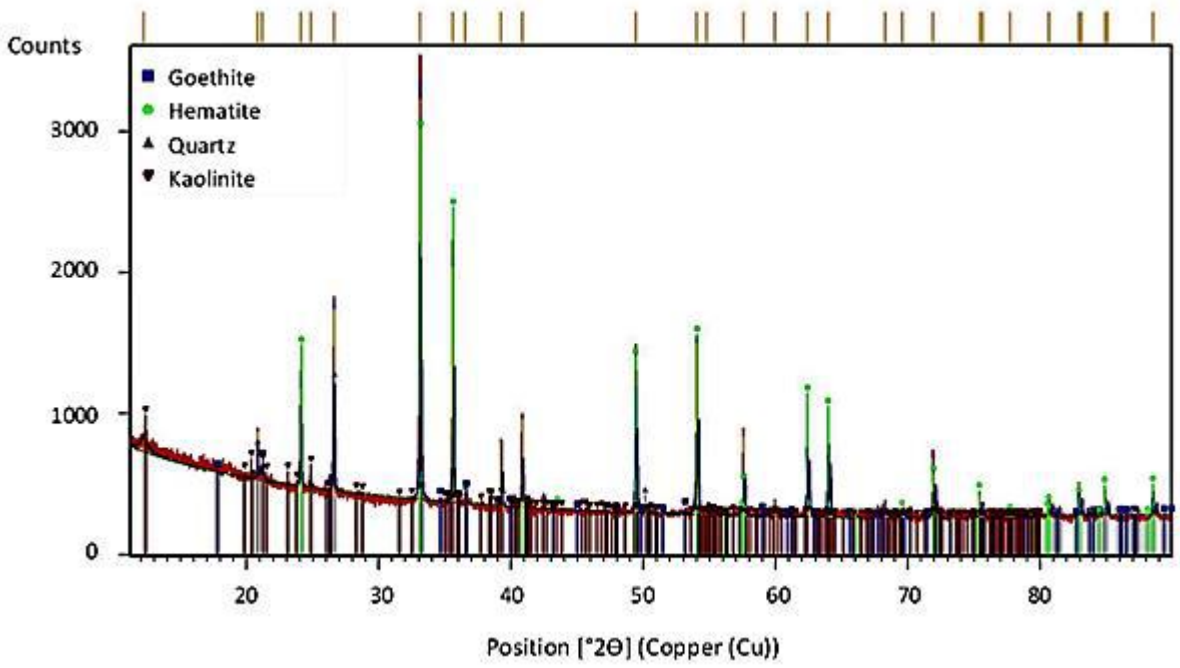

Source: Authors' own elaboration (modified from the instrument output).

Majority presence of hematite (green peaks) and goethite (blue peaks) can be observed in the diffractogram. These results confirm the thermogravimetric analysis regarding the possible minerals found in the sample, and indicate the presence of quartz in the sample.

Figure 7 shows the X-ray diffractogram for the dolomite sample, which identified only dolomite in the sample.

Figure 7 — X-ray diffraction analysis of the dolomite sample.

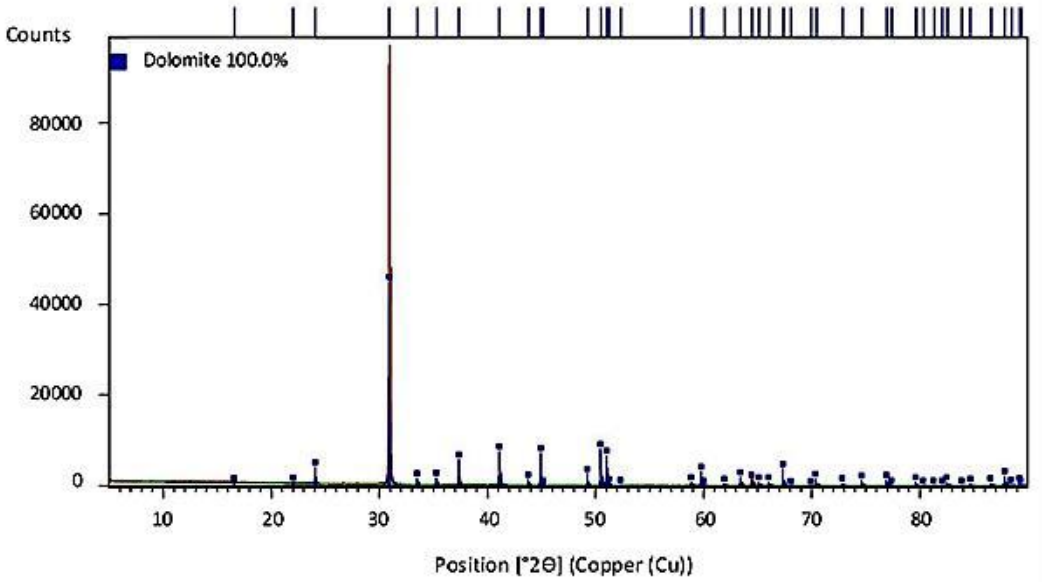

Source: Authors' own elaboration (modified from the instrument output).

Although the thermogram analysis indicated the possible presence of clay minerals, the X-ray diffratometry did not confirm this assumption and as can be seen by the presence of only one type of peak (blue), the material used only presented the presence of dolomite.

3.2 Calibration curve

Figure 8 shows the calibration curve constructed for hematite grade for the image analysis method.

Figure 8 — Calibration curve for hematite grade (samples: 0.1 g).

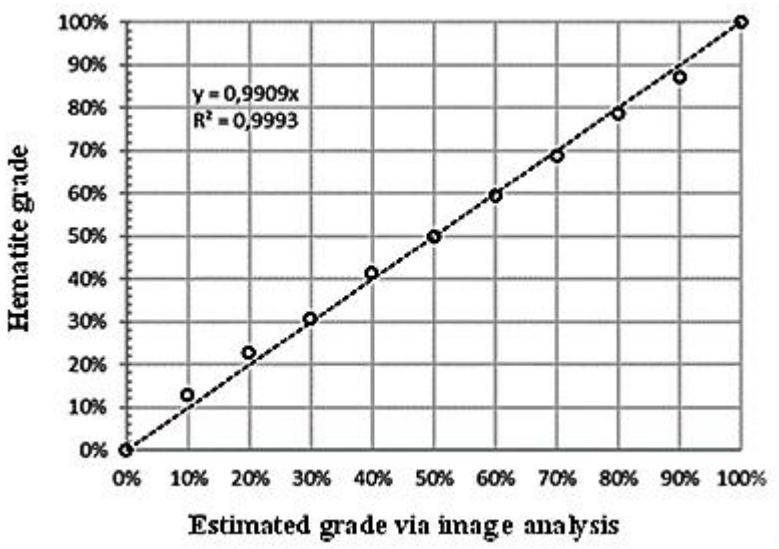

Source: Authors' own elaboration.

As can be seen in the calibration curve, the grades found through the histogram in relation to the actual values are very close, showing a linear correlation with determination coefficient of 99.93 %.

3.3 Microflotation tests

Tables 1 and 2 shows the values of hematite grades in the floated and non-floated material inserted in the algorithm (raw data before data reconciliation).

Table 1 — Grade determination concerning microflotation with saponified oleic acid.

	Image analysis		**Pycnometry**		**Calcination**	
pH	*Floated*	*Non-floated*	*Floated*	*Non-floated*	*Floated*	*Non-floated*
5.0	30.16 %	64.74 %	43.24 %	53.78 %	43.35 %	56.44 %
6.1	41.78 %	51.49 %	45.62 %	54.00 %	46.07 %	50.12 %
7.2	46.21 %	49.79 %	52.15 %	46.81 %	44.06 %	52.24 %
8.3	44.05 %	51.89 %	51.96 %	46.11 %	47.02 %	51.98 %
9.4	27.86 %	64.24 %	23.26 %	75.84 %	36.37 %	61.57 %

Source: Authors' own elaboration.

The results indicate hematite concentration in the non-floated material, mostly at pH 5 and 9.4. Furthermore, at pH 5.0 and pH 6.1 the values of the pycnometry and calcination methods tend to be closer, whereas at pH 7.2 and pH 8.3 the proximity is found between the image analysis method and calcination.

Table 2 — Grade determination concerning microflotation with saponified cottonseed oil.

	Image analysis		**Pycnometry**		**Calcination**	
pH	*Floated*	*Non-floated*	*Floated*	*Non-floated*	*Floated*	*Non-floated*
5.0	36.56 %	63.71 %	31.55 %	56.14 %	45.49 %	52.28 %
6.1	34.81 %	55.72 %	38.59 %	50.76 %	49.10 %	48.98 %
7.2	39.73 %	62.54 %	42.59 %	55.37 %	50.69 %	46.54 %
8.3	45.71 %	52.08 %	36.58 %	62.89 %	34.29 %	63.62 %
9.4	40.51 %	56.08 %	35.19 %	61.82 %	46.35 %	51.84 %

Source: Authors' own elaboration.

For cottonseed oil, the methods of image analysis and pycnometry were the ones that presented the closest results, at pH 5, 6.1 and 7.2. Hematite was also concentrated in non-floated material, but its values tended to be higher at pH 5 and 8.3.

In general, both collectors showed low hematite grades in the floated material. These results indicate that in the floated material there is a higher concentration of dolomite than hematite. Taking into account the results obtained, the possibility for adoption of an anionic reverse flotation circuit can be carefully considered.

The Table 3 and Table 4 show the metallurgical recovery and the Gaudin selectivity index (SI) of hematite, depending on whether one is considering direct flotation route for hematite (and dolomite depression) or reverse flotation route (with depression of hematite and flotation of dolomite).

Table 3 — Metallurgical recovery and SI of the microflotation with saponified oleic acid.

	Metallurgical recovery		**SI**	
pH	*Floated*	*Non-floated*	*Direct route*	*Reverse route*
5	38.79 %	61.21 %	0.67	1.50
6.1	44.25 %	55.75 %	0.84	1.19
7.2	39.39 %	60.61 %	0.97	1.03
8.3	49.93 %	53.07 %	0.97	1.03
9.4	32.88 %	67.12 %	0.41	2.47

Source: Authors' own elaboration.

The metallurgical recovery in the floated material was low at all pH, which can be confirmed by the values of the selectivity index in the direct and reverse routes. In this case, the best recovery was at pH 5 and 9.4 considering the reverse route. However, it must be emphasized that a microflotation campaign does not have as its primary and direct goal the optimization of the circuit, in terms of metallurgical recovery and product contents. This goal is, as a rule, reserved for the subsequent stages of flotation at bench and pilot scale, when developing a new ore processing route.

Table 4 — Metallurgical recovery and SI of the microflotation with saponified cottonseed oil.

	Metallurgical recovery		**SI**	
pH	*Floated*	*Non-floated*	*Direct route*	*Reverse route*
5	51.43 %	48.57 %	0.64	1.57
6.1	53.26 %	46.74 %	0.75	1.33
7.2	40.96 %	59.04 %	0.79	1.26
8.3	30.03 %	69.97 %	0.62	1.61
9.4	39.71 %	60.29 %	0.66	1.51

Source: Authors' own elaboration.

As with oleic acid, the reverse route has higher selectivity index values. The difference is due to the metallurgical recovery values which, in this case, are higher at pH 8.3 and 9.4 in the non-floated material.

The results of the Tables 3 and 4 show, in most cases, a higher value of the metallurgical recovery and Gaudin selectivity index in the non-floated material. These numbers contribute for the consideration that the system is an anionic reverse flotation. Although these parameters are effectively adjusted in the bench flotation phase, such information was calculated to verify the interaction of the reagents with the mineral particles and not the operational optimization.

The results of the adjusted hematite grades for both saponified collectors are illustrated in Figures 9 and 10, along with the actual grades determined by each method.

Figure 9 — Hematite grades in the floated material as a function of pH.

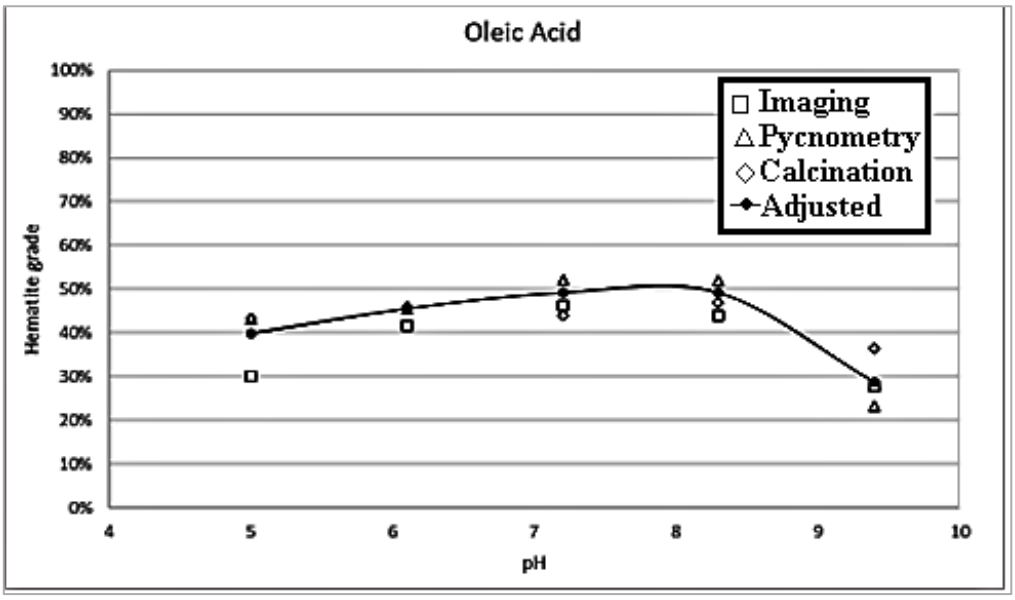

Source: Authors' own elaboration.

As can be seen in Figure 9, at pH 5 and 9.4 the greatest discrepancy of values between some methods and the value adjusted by the algorithm is found. Furthermore, the image analysis method tends to present grades that are farther from the adjusted grade.

Figure 10 — Hematite grades in the floated material as a function of pH.

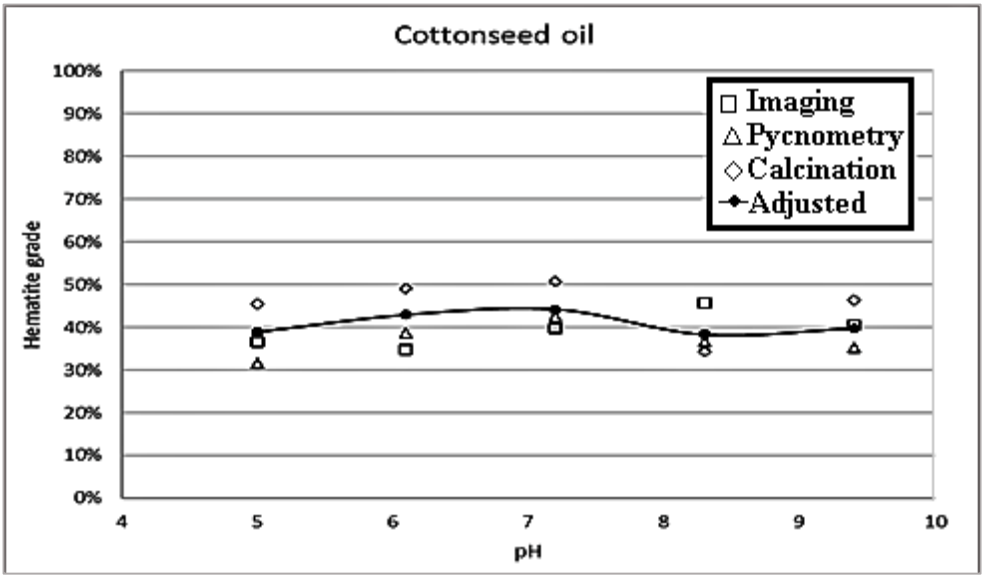

Source: Authors' own elaboration.

In this case, there was a greater variation in the contents of the methods in relation to the adjusted content, mainly calcination and image analysis.

The results of Figure 9 and 10 indicate a variation in the values found by each method that can be justified by the sensitivity of each one during the process. For the oleic acid, the results of pycnometry and calcination were closer. For cottonseed oil, the data tended to disperse more, with some values close between pycnometry and image analysis.

To be used in imaging process, the method of dispersion in very fine particles does not present a good efficiency and requires more caution. The finer the particles are, the greater the tendency to form lumps. In addition, the hematite ultrafine particles have a lighter color, which makes it difficult to distinguish them from the colors of the dolomite in the picture. Therefore, the procedure would be much better applied to coarser particles.

The pycnometry and calcination methods requires attention in weighing since the equations used demand maximum precision so that the values do not deviate from the real.

Regarding the algorithm, it can be noticed its adjustment according to the values used for the calculations, tending to the results of pycnometry and calcination, since they are methods more accurate than image analysis.

More detailed studies of the microflotation process are suggested, with a greater number of variables in order to determine the relative error of each method to increase the reliability of the results. In addition, the implementation of improvements in the image analysis methodology, such as the use of coarser materials, determining the morphometric features of the particles, improving the way particles are dispersed to use a more representative sample quantity.

4. Conclusion

Although the hematite contents recovered for both oils did not present significant results, cottonseed oil can be considered a potential collector at alkaline and acid pH, if a reverse anionic flotation rout is adopted. By way of clarification, it should be emphasized here that at the current stage of the research reported here, no attempt has been made to selectively depress one of the minerals with the addition of a depressant (such as starch, sodium hexametaphosphate, quebracho, tannin, and many others), which would most likely lead to a much greater contrast in the selectivity window, under the studied pH range.

In addition to the incremental contribution to the knowledge of the hematite/dolomite system in the context of froth flotation, this paper has categorically evidenced that the accuracy of simple analytical approaches in binary systems in microflotation can be enhanced by redundant data compatibility algorithms, resulting in process parameters with more reliable values.

Analyzing the procedures separately, it is noticed that pycnometry and calcination tend to be more reliable, since they are intrinsically linked to conventional quantification techniques, however they are quite sensitive in relation to the weighing of materials.

As far as image analysis is concerned, even though this method poses greater challenges in the implementation of the procedure, it shows promise in quantifying the contents of binary samples. However, the use of coarser grained minerals is indicated in order to facilitate the grains separation/individualization and image treatment. In addition, as a recommendation for caution in its use, the morphometric features of the particles (especially their lamellarity) should be preventively determined, so as not to cause statistical bias when quantifying the masses through the areas projected by the particles. Anyway, these morphometric differences can be accounted for by using a calibration curve (with samples of known contents).

Of course, for a better use of the algorithm, it is necessary to use more precise information, such as the actual relative errors of each method. In general, with less uncertain information, the application of the algorithm can be advantageous to obtain results that converge to a theoretical value as close as possible to the real one.

As a final remark, as a suggestion for future research in continuity with this work, the methodological extrapolation to include, for instance, magnetic separation (or the sample magnetic susceptibility) is recommended. In addition, the careful survey of the metrological uncertainties of each of these expeditious analysis methods will increase the result reliability for the redundant data reconciliation algorithm used here.

Acknowledgments

The authors are thankful to Brazilian Council for Technological and Scientific Development (CNPq), Foundation for Research Support of the State of Minas Gerais (FAPEMIG), and Brazilian Federal Agency for Support and Evaluation of Graduate Education (CAPES), for their financial support. They also are grateful to technicians from Mining Engineering Department at UFOP, for their experimental and logistic invaluable help. The authors also take the opportunity to declare that there is no conflict of interest regarding the publication of this article.

References

Aliyu1, W. A., Hossain, Md. I., & Specht, E. (2022) Numerical Approach in Determination of Thermophysical Material Properties in Decomposition of Lumpy Dolomite Particles. *Proceedings of the 9th International Conference on Fluid Flow, Heat and Mass Transfer (FFHMT'22*), Niagara Falls, Canada. 198. 10.11159/ffhmt22.198

Brandão, P. R. G., Caires, L. G., & Queiroz, D. S. B. (1994). Vegetable lipid oil-based collectors in the flotation of apatite ores. *Minerals Engineering*. 7(7); 917-925.

Chudacek, M. W., Fichera, M. A., Rosa, M. D., & Silva, R. V. G. (1992). Flotation testing: from pure minerals to real ores. *In: encontro nacional de tratamento de minérios e hidrometalurgia*.

Costa, D. S. (2012). *Uso de óleos vegetais amazônicos na flotação de minérios fosfáticos*. PhD Thesis. Universidade Federal de Minas Gerais, Belo Horizonte. David, P. Shoemaker, D. P., Garland, C.W., & Nibler, J. W. (1996). Experiments in Physical Chemistry (Sixth Edition). McGraw-Hill: New York, 1996. xii + 778 pp. ISBN 0-07-057074-4.

Drzymala, J. (1994a). Characterization of materials by Hallimond tube flotation. Part 1: maximum size of entrained particles. International Journal of Mineral Processing, 42(3-4), 139-152. https://doi.org/10.1016/0301-7516(94)00036-0

Drzymala, J. (1994b). Characterization of materials by Hallimond tube flotation. Part 2: maximum size of floating particles and contact angle. International Journal of Mineral Processing, 42 (1994) 153-167.

Erhan, S. Z. (2005). *Industrial uses of vegetable oils. Champaign*, Illinois: American Oil Chemists' Society.

Fuerstenau, M. C. (1964). An improved micro-flotation technique. *Engineering and Mining Journal*; 165(11);108-9.

Gaudin, A. M. (1975). *Principles of Mineral Dressing*. New Delhi: Tata McGraw-Hill. xi, 554 pages, il.

Hodouin, D. (2010). Process Observers and Data Reconciliation Using Mass and Energy Balance Equations. In: Sbárbaro, D., Del Villar, R. (eds) *Advanced Control and Supervision of Mineral Processing Plants*. *Advances in Industrial Control*. Springer, London. https://doi.org/10.1007/978-1-84996-106-6_2

Leja, J. (2004). *Surface chemistry of froth flotation*, (2aed.) Kluwer Academic/Plenum Publishers.

Leonel, C. M. L. (2011). *Estudo de Processo de Calcinação como Operação Unitária Adicional na Pelotização de Minérios de Ferro com Altos Valores de PPC*. PhD Thesis. Universidade Federal de Minas Gerais. Belo Horizonte.

Luz, J. A. M. (1996). *Flotação Aniônica de Rejeito Itabirítico: Estudo de Reagentes Alternativos e Modelamento Polifásico do Processo*. PhD Thesis. Universidade Federal de Minas Gerais. Belo Horizonte.

Luz, J. A. M. (1999). Uso de vazões na compatibilização de teores via multiplicadores de Lagrange. *Revista Escola de Minas – REM;* 5(4); 269-274.

Luz, J. A. M. (2016). Flotation of Iron Ore. In: Colás, R., Totten, G. E. (Ed.). *Encyclopedia of Iron, Steel, and Their Alloys*. Taylor & Francis, 2016, v.2, p. 1249-1288.

Milhomem, F. O. (2020). Cinética De Flotação No Sistema Hematita E Quartzo Com Uso De Óleos Vegetais. Phd Thesis. Universidade Federal De Ouro Preto, Ouro Preto.

Milhomem, F. O., & Luz, J. A. M. (2018). Colorimetric Image Analysis for Hematite Grade Estimation. *Journal of Materials Education;* 40; 155-162.

Millan, N. M., *et al.* (2016). Associação dos resultados de análise térmica e análise química de amostra de dolomita natural. *In: X Congresso Brasileiro e IV Congresso Pan Americano de análise térmica e calorimetria*. São Paulo, Brasil.

Neuppmann, P. H. (2019). *Enriquecimento de finos hematíticos via flotação por carreador*. Masters Thesis. Universidade Federal de Ouro Preto, Ouro Preto, 2019.

Rocha, G. M., Gonçalves, G. M. C., Ramos, K. S., Cota, T. G., & Lima, R. M. F. (2009). Caracterização física, química e mineralógica de uma amostra de minério de ferro de Brucutu. *Tecnologia em Metalurgia, Materiais e Mineração*, 16 (1); 88-94.

Rocha, J. M. P. (2008). *Definição da tipologia e caracterização mineralógica e microestrutural dos itabiritos anfibolíticos das minas de Alegria da Samarco Mineração S.A*. PhD Thesis. Universidade Federal de Minas Gerais, Belo Horizonte.

Salama, W., Aref, M. E., & Gaupp, R. (2015). Spectroscopic characterization of iron ores formed in different geological environments using FTIR, XPS, Mössbauer spectroscopy and thermoanalyses. Spectrochimica *Acta Part A: Molecular and Biomolecular Spectroscopy*. 136, part C, 1816 – 1826.

Sampaio, J. A., & Almeida, S. L. M. (2008). Calcário e dolomito. *In: Rochas e Minerais Industriais no Brasil: usos e especificações*. (2a ed.): CETEM/MCTI, 363-387.

Silva, A. C., Silva E. M. S., Silva, T. C., & Alves, B. E. (2015). Apatite microflotation using pequi oil. *Mineral Processing and Extractive Metallurgy,* 124(4); 233-239.

Soares, R. A. L., Nascimento, R. M., Paskocimas, C. A., & Castro, R. J. S. (2014). Avaliação da adição de dolomita em massa de cerâmica de revestimento de queima vermelha. *Cerâmica*, 90, 516 – 523.

Souza, M. O. G., Santos, M. V. R., Castro, L. M. F., & Silva, C. P. (2020). Production and in situ transformation of hematite into magnetite from the thermal decomposition of iron nitrate or goethite mixed with biomass. *Journal of Thermal Analysis and Calorimetry*. 139, 1731 – 1739.

Vasebi, A., Poulin, E., & Hodouin, D. (2012). Dynamic data reconciliation in mineral and metallurgical plants. Annual Reviews in Control 36 (2012) 235–243.

Vieira, M., Lédo, P. G. S., Lima, R. F. S., Paulo, J. B. A., & Brandão, P. R. G. (2005). Flotação de calcita a partir de óleos vegetais regionais saponificados como agentes coletores. *In: Anais do 6º Congresso Brasileiro de Engenharia Química em Iniciação Científica*. Campinas, Brasil. Campinas: UNICAMP, 1-5.

Wills, B. A., & Napier–Munn, T. (2006). *Mineral Processing Technology: An Introduction to the Practical Aspects of Ore Treatment and Mineral Recovery*. (7a. ed.): Elsevier Science e Technology Books, 450 p.